An Improved Method for Rapid and Efficient Radioiodination of Iodine-123-IQNB

Kan Sam Lee, Xiao-shu He, Douglas W. Jones, Richard Coppola, Julia G. Gorey, Michael B. Knable, Brian R. deCosta, Kenner C. Rice and Daniel R. Weinberger

Clinical Brain Disorders Branch, National Institute of Mental Health (NIMH), National Institutes of Health (NIH), NIMH Neuroscience Center at St. Elizabeths, Washington, D.C.; and Laboratory of Medicinal Chemistry, National Institute of Diabetes and Digestive and Kidney Diseases, NIH, Bethesda, Maryland

The SPECT radioligand, 3-quinuclidinyl-4-[^{123}I]iodobenzilate ([^{123}I]IQNB), binds to muscarinic receptors and has generated interest as a potential agent for clinical SPECT. Unfortunately, cumbersome and inefficient radioiodination procedures have limited the practicality of [^{123}I]IQNB SPECT imaging. **Methods:** We report a rapid (5 min) and simple radioiodination procedure for preparing [^{123}I]IQNB from a tri-n-butylstannyl precursor in a no-carrier-added reaction that yields high specific activity with radiochemical yield exceeding 60%. The radiochemical purity of the final product exceeds 95%. **Results:** We have used this procedure to radioiodinate the four stereoisomers of [^{123}I]IQNB. The procedure is highly reliable and reproducible. SPECT studies on a healthy human volunteer at 1, 2, 6 and 24 hr after injection of each of the four stereoisomers reveal expected differences in the kinetic and binding characteristics of the four stereoisomers. (R,S)-[^{123}I]IQNB appears to be the SPECT agent of choice. **Conclusion:** Radioiodination of [^{123}I]IQNB from our tri-n-butylstannyl precursor is simpler, more efficient and less expensive than previous techniques. The potential exists for a "kit" which would be practical in a typical clinical setting.

Key Words: iodine-123-IQNB; diastereomers; muscarinic receptors; SPECT

J Nucl Med 1996; 37:2021–2024

The radioligand, 3-quinuclidinyl-4-iodobenzilate (IQNB), is a potent muscarinic receptor antagonist. As [^{125}I]IQNB, it has been used in numerous animal studies and postmortem studies of the distribution of muscarinic receptors in brain and other tissue (*1–13*). As [^{123}I]IQNB, it has also been used successfully as a SPECT radioligand in studying the relative distribution of muscarinic receptors in patients with Alzheimer's disease (*14–21*). A difficulty with this radioligand, however, has been the problem of labeling the phenyl ring of quinuclidinyl benzilate (QNB) in reactions with ^{125}I or ^{123}I sodium iodide (NaI). Several radioiodination methods have been reported; among these are trifluoroacetic acid assisted direct radioiodination of QNB (*22*), a modification of the Wallach triazene method (*23,24*), copper(I) assisted nucleophilic aromatic exchange (*20,25*) and a QNB-boronic acid method (*26*). A commercial kit based on an exchange reaction is also available. Since the four stereoisomers of [^{123}I]IQNB (Fig. 1) display different binding characteristics, isomeric purity is a concern, and, thus far, only triazene and exchange methods have successfully prepared isomerically and radiochemically pure (R,S)-[^{123}I]IQNB. Unfortunately, both methods have disadvantages: for example, the triazene reaction requires 90 min and has low radiochemical yield and the exchange reaction requires 120 min and yields low specific activity, typically well below 37 TBq/mmole (1000 Ci/mmole). To address these difficulties, we have developed a simpler, faster and more efficient technique for preparing [^{123}I]IQNB from isomerically pure stannylated-QNB precursors.

Received Oct. 16, 1995; revision accepted Jan. 28, 1996.

For correspondence or reprints contact: Kan Sam Lee, PhD, Clinical Brain Disorders Branch, NIMH, Neuroscience Center at St. Elizabeths, 2700 Martin Luther King, Jr. Ave., S.E., Washington, D.C. 20032.

MATERIALS AND METHODS

Isomerically pure tri-n-butylstannyl-QNB precursors of the four [^{123}I]IQNB stereoisomers (Fig. 1) were prepared in advance and their structure and isomeric purity were confirmed by nuclear magnetic resonance (NMR) and x-ray crystallography. The precursors are quite stable when stored at 4°C in ethanol (1 mg/ml; 1.6 m*M*). Radioiodination begins by mixing 50 μl (80 nmole) tri-n-butylstannyl-QNB solution and 200 μl ethanol with 370 Mbq to 1110 MBq (10 mCi to 30 mCi) dry, carrier-free [^{123}I]NaI in a sealed vial. To neutralize the pH, 40 μl to 300 μl 1N hydrochloric acid (HCl) is added depending upon the specified sodium hydroxide (NaOH) content of each [^{123}I]NaI vial. Adding 100 μl aqueous peracetic acid (0.32% w/v) initiates the reaction which continues for 5 min at room temperature (Fig. 2). To quench the reaction, 20 mg sodium bisulfite ($NaHSO_3$) is added, and addition of 25 mg sodium hydrogen carbonate ($NaHCO_3$) makes the mixture basic.

Ethyl acetate extraction (3 × 1 ml) separates [^{123}I]IQNB from the reaction mixture. The combined ethyl acetate extracts are washed with 1 ml of water, then evaporated to dryness under a nitrogen stream. The dry residue is reconstituted in 200 μl ethanol and purified by high performance liquid chromatography (HPLC) on a reverse-phase C-18 column. Isocratic elution proceeds at 1 ml/min with methanol:water:formic acid (600:400:1) in 1 mg/ml 1-octanesulfonic acid, sodium salt. The fraction containing [^{123}I]IQNB is extracted with ethyl acetate (3 × 1 ml). Evaporating the combined extracts to dryness under a nitrogen stream yields the purified [^{123}I]IQNB radioligand, which is prepared for injection by reconstitution in 200 μl ethanol and addition of 2 ml sterile 0.9% saline solution. A 0.22-μm syringe filter sterilized the solution, and each preparation was tested for pyrogenicity and sterility.

The radiochemical yield was determined by dividing the activity of the final injectable product by initial activity of [^{123}I]NaI, each determined by a dose calibrator. Radiochemical purity was determined by thin-layer chromatography (TLC) using a methanol:chloroform (85:15) solvent system on silica gel plates. Plates were co-spotted with nonradioactive IQNB standard. After drying, the radioactive lane was counted with an imaging scanner. The [^{123}I]IQNB peak was confirmed by comparison with the cold-IQNB fluorescence peak, and integrated counts under this peak were then divided by the total integrated counts for the entire lane to determine radiochemical purity.

Specific activity was determined for a batch of (R,S)-[^{123}I]IQNB by saturation binding analysis with cloned M_2 muscarinic receptors. Assays were performed in six 1 ml volumes of Tris-HCl (50 m*M*, pH 7.4) incubation buffer

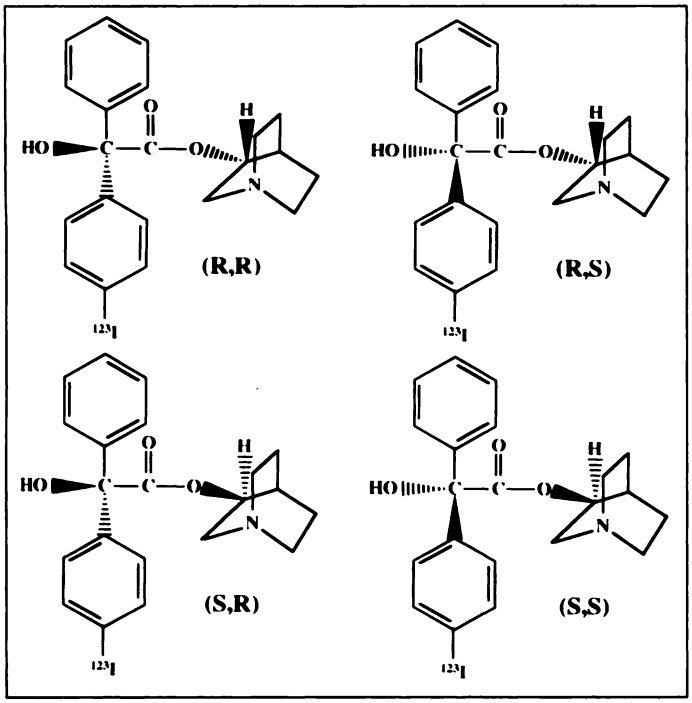

FIGURE 1. Chemical structures of the four stereoisomers of [^{123}I]IQNB are shown. In the top row are (R,R)-[^{123}I]IQNB (left) and (R,S)-[^{123}I]IQNB (right), both are potent mucarinic antagonists based on (R)-QNB. (S, R)-[^{123}I]IQNB (left) and (S,S)-[^{123}I]IQNB (right), the less potent enantiomers based on (S)-QNB, are in the bottom row.

containing NaCl (120 m*M*), $CaCl_2$ (2 m*M*), KCl (5 m*M*) and $MgCl_2$ (1 m*M*). Each volume consisted of 80. 8 p*M* (B_{max}) M_2 receptors and (R,S)-[^{123}I]IQNB in concentrations from 74 Kbq/ml to 2 KBq/ml (2 μCi/ml to 60 nCi/ml) in successive 2:1 dilutions. Six identically prepared volumes included 10 μM atropine to determine nonspecific binding. The reaction was initiated by addition of the receptors and incubated for 30 min at 37°C. Receptors were isolated by filtration with 3 × 3 ml rinses of ice-cold Tris-HCl buffer (pH 7.4 at 25°C) across a Whatman GF/B glass filter, presoaked in polyethyleneimine (0.1%), using a 24-well filtration device. A gamma counter assayed the filters and radioligand aliquots. Weighted nonlinear regression analysis determined the specific activity and the equilibrium dissociation constant (K_d) from these data.

SPECT imaging studies were performed with the four stereoisomers of [^{123}I]IQNB in a healthy 31-yr-old male volunteer who gave written informed consent under a protocol approved by the National Institute of Mental Health Institutional Review

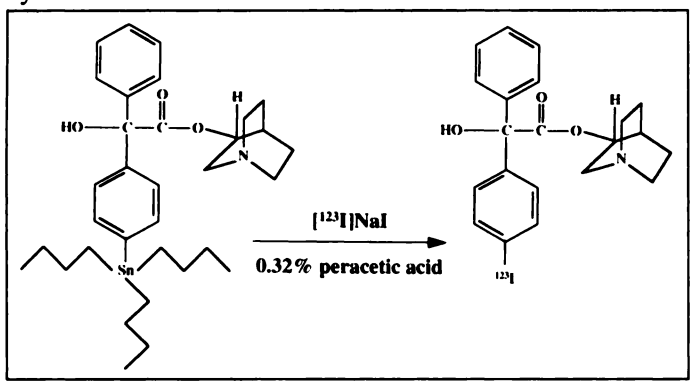

FIGURE 2. Schematic diagram summarizes the radioiodination reaction. The tri-n-butylstannyl-QNB precursor (left) is reacted with [^{123}I]NaI in the presence of 0.32% peracetic acid at room temperature for 5 min. The tri-n-butylstannyl group is exchanged with ^{123}I to generate [^{123}I]IQNB (right).

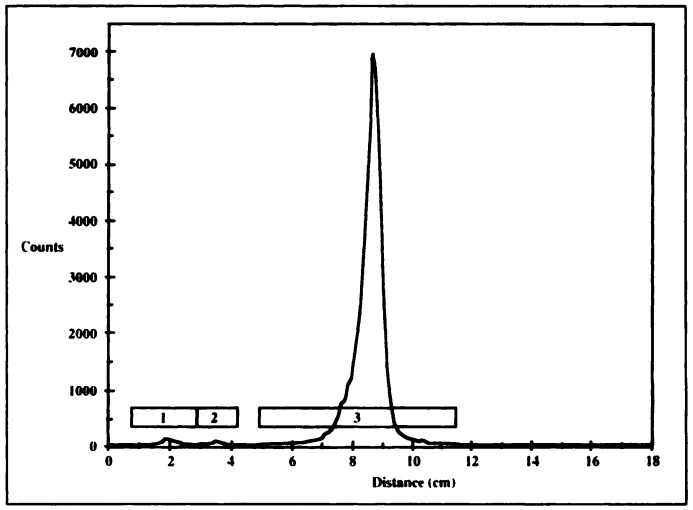

FIGURE 3. Representative TLC chromatogram illustrates high radiochemical purity of [^{123}I]IQNB generated by the tri-n-butylstannyl-QNB method after HPLC purification.

Board. At least 3 wk separated the four injections, and the final session was about 4 mo after the first. In each session, approximately 37 MBq (10 mCi) of [^{123}I]IQNB in a pure stereoisomeric form was injected intravenously. Lugol's solution (five drops daily) was administered one day before injection and for the following three days to block thyroid uptake. A Ceraspect camera (Digital Scintigraphics, Waltham, MA) performed 30 min SPECT acquisitions at 1, 2, 6 and 24 hr postinjection with a high-resolution (7.5 mm FWHM) collimator in 120-projection step-and-shoot mode. The photopeak (145–175 keV) and two windows used for scatter correction (127–143 keV and 175–191 keV) were acquired. Reconstruction by backprojection with a tenth order Butterworth filter (1 cm cutoff) generated an isotropic volume (1.67 mm voxels) of 64 128×128 transverse slices. The Ceraspect software corrected for attenuation (coefficient 0.150/cm).

RESULTS

Preparation of [^{123}I]IQNB from isomerically pure tri-n-butylstannyl-QNB precursors proved reliable and efficient. For all isomers, radiochemical yields fell consistently in the range of 60% to 70%, and radiochemical purities typically exceeded 95% (Fig. 3). The saturation binding assay indicated a high-specific activity of 290 TBq/mmole (7900 Ci/mmole) and a K_d of 0.074 n*M* for (R,S)-[^{123}I]IQNB with M_2 receptors (Fig. 4). The cloned receptors had extremely low nonspecific binding and proved to be an accurate and convenient tool for specific activity determination.

Figure 5 shows representative SPECT images at a transverse level bisecting the thalamus inferior to the genu of the corpus callosum and superior to the cerebellum. These images have been corrected for injected dose, but not for radioactive decay. Thus, all images are displayed on the same relative scale and reflect the actual count rates observed at the times postinjection. Although (R,S)-[^{123}I]IQNB and (R,R)-[^{123}I]IQNB display generally similar characteristics, (R,S)-[^{123}I]IQNB has a greater retention at all times and substantially more at 24 hr. In fact, continued overnight uptake essentially offsets radioactive decay. The (S,R)-[^{123}I]IQNB and (S,S)-[^{123}I]IQNB images are consistent with an absence of specific binding and, presumably, these low levels reflect nonspecific uptake mediated by blood flow, permeability and tissue diffusion. These images are probably indicative of the nonspecific component of (R,S)-[^{123}I]IQNB and (R,R)-[^{123}I]IQNB images which appear domi-

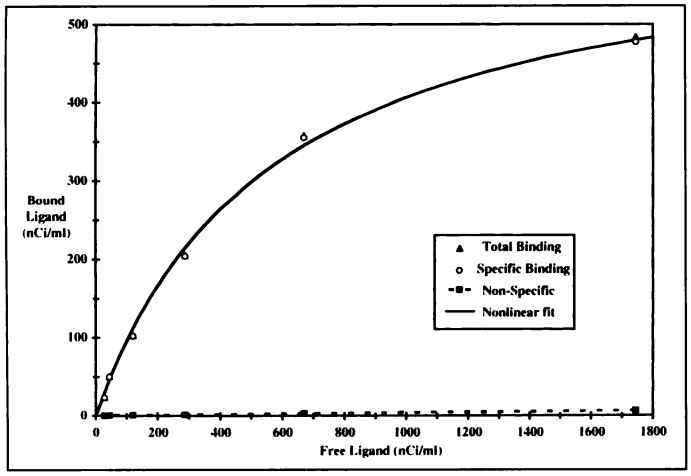

FIGURE 4. Data and fitted curve for the saturation binding assay are shown. Specific binding of radioligand to receptors (○) was obtained by subtracting the nonspecific binding (-■-) from the total binding (▲). The solid line is the fitted specific binding curve from the weighted nonlinear regression analysis.

nated by specific receptor binding. This is particularly true in 6 hr and 24 hr data. By 6 hr postinjection, the specific-to-nonspecific ratio appears high enough to generate potentially useful clinical data. The cerebellum, another nonspecific component indicator, also exhibits extremely low count rates by this time. For both (R,S)-[^{123}I]IQNB and (R,R)-[^{123}I]IQNB, the high retention in basal ganglia and cortical regions and the lesser uptake in thalamus seems consistent with binding predominantly to M_1 subtype muscarinic receptors. Differences between the images with these two isomers is most likely explained by differing affinities rather than by varying subtype selectivity.

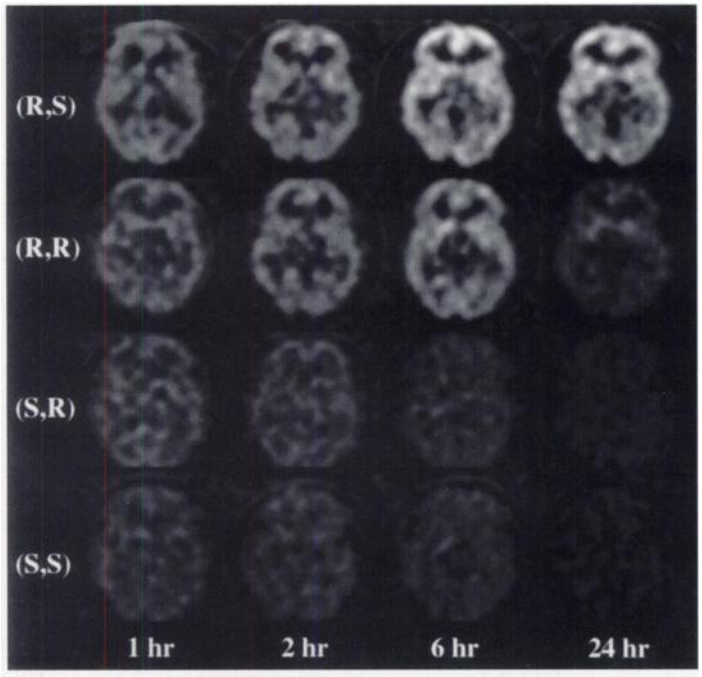

FIGURE 5. SPECT images of the four stereoisomers of [^{123}I]IQNB in the same normal volunteer. Three 30-min acquisitions were performed on the first day (1, 2 and 6 hr postinjection); a single 30-min scan was acquired at 24 hr. The scans have been normalized to injected dose, but they have not been corrected for decay. Thus, the images reflect actual relative counting rates at the various times.

DISCUSSION

Our tri-n-butylstannyl-QNB method substantially simplifies radioiodination of [^{123}I]IQNB. The high-efficiency reaction greatly reduces [^{123}I]NaI requirements and, thus, the expense of SPECT studies. Radiochemical yields of the 5 min reaction consistently exceed those of triazene and exchange methods which require reaction times of 90 min and 120 min, respectively. Additionally, the tri-n-butylstannyl-QNB method yields a very high specific activity radioligand.

As expected, the stereoisomers differed substantially in SPECT imaging with (R,S)-[^{123}I]IQNB being the SPECT agent of choice, and (R,R)-[^{123}I]IQNB also being possibly useful on the day of injection. (S,S)-[^{123}I]IQNB and (S,R)-[^{123}I]IQNB appear to be of little potential value except, perhaps, as a nonspecific uptake measure, but this use requires quantitative validation.

The tri-n-butylstannyl-QNB method simplifies the preparation of [^{123}I]IQNB greatly and has potential as a "kit" with practicality in a typical clinical setting. The HPLC portion of the procedure would need to be eliminated, and a simpler, yet equally reliable, purification method would be required. We are currently pursuing this problem.

ACKNOWLEDGMENT

We thank Aaron Deveny, PhD, for technical assistance with the saturation binding analysis.

REFERENCES

1. Gibson RE, Rzeszotarski WJ, Jagoda EM, Francis BE, Reba RC, Eckelman WC. Iodine-125 3-quinuclidinyl 4-iodobenzilate: a high affinity, high specific activity radioligand for the M1 and M2-acetylcholine receptors. *Life Sci* 1984;34:2287–2296.
2. Gibson RE, Weckstein DJ, Jagoda EM, Rzeszotarski WJ, Reba RC, Eckelman WC. The characteristics of iodine-125 4-IQNB and H-3 QNB in vivo and in vitro. *J Nucl Med* 1984;25:214–222.
3. Eckelman WC, Eng R, Rzeszotarski WJ, Gibson RE, Francis B, Reba RC. Use of 3-quinuclidinyl 4-iodobenzilate as a receptor binding radiotracer. *J Nucl Med* 1985; 26:637–642.
4. Gibson RE, Schneidau TA, Cohen VI, et al. In vitro and in vivo characteristics of [iodine-125] 3-(R)-quinuclidinyl (S)-4-iodobenzilate. *J Nucl Med* 1989;30:1079–1087.
5. Sawada Y, Hiraga S, Francis B, et al. Kinetic analysis of 3-quinuclidinyl 4-[^{125}I]iodobenzilate transport and specific binding to muscarinic acetylcholine receptor in rat brain in vivo: implications for human studies [see comments]. *J Cereb Blood Flow Metab* 1990;10:781–807.
6. Sawada Y, Hiraga S, Patlak CS, Ito K, Pettigrew KD, Blasberg RG. Cerebrovascular transport of [^{125}I]quinuclidinyl benzilate, [^{3}H]cyclofoxy and [^{14}C]iodoantipyrine. *Am J Physiol* 1990;258:H1585–H1598.
7. Gibson RE, Moody T, Schneidau TA, Jagoda EM, Reba RC. The in vitro dissociation kinetics of (R,R)-[^{125}I]4-IQNB is reflected in the in vivo washout of the radioligand from rat brain. *Life Sci* 1992;50:629–637.
8. Gitler MS, Cohen VI, De la Cruz R, et al. A novel muscarinic receptor ligand which penetrates the blood brain barrier and displays in vivo selectivity for the m2 subtype. *Life Sci* 1993;53:1743–1751.
9. Hiramatsu Y, Kawai R, Reba RC, Simon TR, Baum BJ, Blasberg RG. Kinetic analysis of rat parotid gland muscarinic receptors in vivo: comparison with brain and heart. *Am J Physiol* 1993;264:G541–G552.
10. Gitler MS, De la Cruz R, Zeeberg BR, Reba RC. Tritiated QNB displays in vivo selectivity for the m2 subtype. *Life Sci* 1994;55:1493–1508.
11. Hiramatsu Y, Eckelman WC, Baum BJ. Interaction of iodinated quinuclidinyl benzilate enantiomers with M3 muscarinic receptors. *Life Sci* 1994;54:1777–1783.
12. Hiramatsu Y, Kawai R, Reba RC, Blasberg RG, Baum BJ. Kinetic analysis of rat exocrine gland muscarinic receptors in vivo. *J Pharmacol Exp Ther* 1994;269:1205–1212.
13. Hiramatsu Y, Eckelman WC, Carrasquillo JA, et al. Kinetic analysis of muscarinic receptors in human brain and salivary gland in vivo. *Am J Physiol* 1995;268:R1491–R1499.
14. Eckelman WC, Reba RC, Rzeszotarski WJ, et al. External imaging of cerebral muscarinic acetylcholine receptors. *Science* 1984;223:291–293.
15. Holman BL, Gibson RE, Hill TC, Eckelman WC, Albert M, Reba RC. Muscarinic acetylcholine receptors in Alzheimer's disease. In vivo imaging with iodine- 123-labeled 3-quinuclidinyl-4-iodobenzilate and emission tomography. *JAMA* 1985;254: 3063–3066.
16. Weinberger DR, Mann U, Gibson RE, et al. Cerebral muscarinic receptors in primary degenerative dementia as evaluated by SPECT with iodine-123-labeled QNB. *Adv Neurol* 1990;51:147–150.
17. Weinberger DR, Gibson R, Coppola R, et al. The distribution of cerebral muscarinic acetylcholine receptors in vivo in patients with dementia. A controlled study with ^{123}IQNB and single photon emission computed tomography. *Arch Neurol* 1991;48: 169–176.

18. Weinberger DR, Jones D, Reba RC, et al. A comparison of FDG PET and IQNB SPECT in normal subjects and in patients with dementia. *J Neuropsych Clin Neurosci* 1992;4:239–248.
19. Weinberger DR, Jones DW, Sunderland T, et al. In vivo imaging of cerebral muscarinic receptors with iodine-123-QNB and SPECT: studies in normal subjects and patients with dementia. *Clin Neuropharmacol* 1992;15:194A–195A.
20. Wyper DJ, Brown D, Patterson J, et al. Deficits in iodine-labeled 3-quinuclidinyl benzilate binding in relation to cerebral blood flow in patients with Alzheimer's disease. *Eur J Nucl Med* 1993;20:379–386.
21. Sunderland T, Esposito G, Molchan SE, et al. Differential cholinergic regulation in Alzhiemer's patients compared to controls following chronic blockade with scopolamine: a SPECT study. *Psychopharmacol* 1995;121:231–241.
22. Lee KS, Gibson RE, Eckelman WC, Reba RC. Radioiodination of a 3-quinuclidinyl benzilate using no-carrier-added concentration of iodine-125/NaI [Abstract]. *J Nucl Med* 1986;27:(suppl)1045P.
23. Rzeszotarski WJ, Eckelman WC, Francis BE, et al. Synthesis and evaluation of radioiodinated derivatives of 1-azabicyclo[2.2.2]oct-3-yl alpha-hydroxy-alpha-(4-iodophenyl)-alpha- phenylacetate as potential radiopharmaceuticals. *J Med Chem* 1984;27:156–160.
24. Cohen VI, Rzeszotarski WJ, Gibson RE, Fan LH, Reba RC. Preparation and properties of (R)-(−)-1-azabicyclo[2.2.2]oct-3-yl- (R)-(+)-alpha-hydroxy-alpha-(4-[^{125}I]iodophenyl)-alpha-phenyl acetate and (R)-(−)-1-azabicyclo[2.2.2]oct-3-yl-(S)-(−)-alpha-hydroxy-alpha- (4-[^{125}I]iodophenyl)-alpha-phenyl acetate as potential radiopharmaceuticals. *J Pharm Sci* 1989;78:833–836.
25. Owens J, Murray T, McCulloch J, Wyper D. Synthesis of (R,R)^{123}I-QNB, a SPECT agent for cerebral muscarinic acetylcholine receptors in vivo. *J Lab Comp Radiopharm* 1991;31:45–60.
26. Kabalka GW, Gai YZ, Mathur S. Synthesis of iodine-125-labeled 3-quinuclidinyl 4′-iodobenzilate. *Int J Rad Appl Instrum [b]* 1989;16:359–360.

Monte Carlo-Based Analysis of PET Scatter Components

Lars-Eric Adam, Matthias E. Bellemann, Gunnar Brix and Walter J. Lorenz
Radiological Diagnostics and Therapy, German Cancer Research Center, Heidelberg, Germany

This study quantifies the different scatter components in PET and examines how the different components degrade reconstructed PET images. **Methods:** We simulated the measurement of various phantoms using Monte Carlo (MC) calculations and compared the MC-generated projections and images with the corresponding experimental data. The coincidences were subdivided in four classes: primaries, object scatter (scattered in the object only), gantry scatter (scattered in the scanner only) and mixed scatter (scattered both in the object and the scanner). **Results:** In the projections of the line sources, the gantry scatter was closely located around the source position, whereas the object scatter was smeared over the whole field of view and could be parameterized well by a monoexponential function. The mixed scatter had nearly the same distribution as the object scatter, but with a smaller amplitude. The calculations and experimental data were in excellent agreement; i.e., led to the same parameterization of the scatter distribution functions and to a similar localization of the scatter components in the reconstructed images. **Conclusion:** The spatial distribution of the scatter components justifies the widely-used assumption that it is sufficient to restrict experimental scatter correction techniques to the object scatter. Furthermore, it is possible to derive the parameters for the scatter kernels, which are needed for the convolution-subtraction algorithm, by MC simulations.

Key Words: PET; scatter components; scatter correction; Monte Carlo simulations

J Nucl Med 1996; 37:2024–2029

The strength of PET is its ability to quantify the activity distribution of radionuclides in the human body. The accuracy of the quantification, however, critically depends upon the adequate correction of the raw data. Major corrections concern the detector efficiency, the dead time, the random coincidences, the scattered radiation and the attenuation in the object. Scatter correction is mandatory, particularly in abdominal imaging. Without scatter correction, the regional activity accumulation can be under- or overestimated and, thus, may lead to false medical interpretations (*1*).

Received Nov. 11, 1995; revision accepted March 3, 1996.
For correspondence or reprints contact: Lars-Eric Adam, MSc, PET Research Group, Radiological Diagnostics and Therapy, German Cancer Research Center (dkfz), Im Neuenheimer Feld 280, D-69120 Heidelberg, Germany.

Our study is focused on the differentiation of the scatter components that result from the object and the gantry. Based on these data, we try to answer the questions as to where the scatter process takes place, which components are dominant, and how they contribute to the images. A powerful tool for such examinations is the Monte Carlo (MC) technique, which simulates real experiments on the computer and distinguishes the coincidences in the desired way. The direct comparison of the simulations with experiments serves as a cross check.

Several studies have been published that address MC simulations of the scatter process in PET (*2–7*). They concern scatter in small animal PET systems (*3–5*) as well as in whole-body tomographs (*6*), and include studies that use the MC simulation as a basis for a PET simulation program (*7*). It is therefore well known how the total scatter contributes to the projections of the measured data. Due to limited computer power available in the past, however, these studies had large statistical errors.

Our study extends the MC simulations to a whole-body tomograph with count numbers that are in the order of the measured data. This makes it possible to reconstruct images of the different scatter components and to deduce the parameters of the scatter kernels from the simulations. These data are needed in scatter-correction algorithms, such as the convolution-subtraction technique (*8,9*).

MATERIALS AND METHODS

PET System

The measurements and simulations were performed for a whole-body PET system (PC 2048–7WB, Scanditronix AB, Uppsala, Sweden). It is a two-ring system with alternating BGO ($Bi_4Ge_3O_{12}$) and GSO (Gd_2SiO_5) detector crystals of $6 \times 20 \times 30$ mm^3. The detector rings are separated by a 5-mm thick lead septum. With the two rings, three slices (two direct and one cross plane) are imaged simultaneously. The patient port diameter is 57 cm, the transaxial field of view (FOV) is 52 cm, and the axial FOV is 4.5 cm. The in-plane resolution in the stationary mode is 6.3 mm in the center of the tomograph and 8.2 mm at a radial distance of 20 cm from the center (*10*).